Laser altimetry reveals complex pattern of Greenland Ice Sheet dynamics

Beata M. Csatho[a,1], Anton F. Schenk[a], Cornelis J. van der Veen[b], Gregory Babonis[a], Kyle Duncan[a], Soroush Rezvanbehbahani[c], Michiel R. van den Broeke[d], Sebastian B. Simonsen[e], Sudhagar Nagarajan[f], and Jan H. van Angelen[d]

[a]Department of Geology, University at Buffalo, Buffalo, NY 14260; Departments of [b]Geography and [c]Geology, University of Kansas, Lawrence, KS 66045; [d]Institute for Marine and Atmospheric Research, Utrecht University, 3584 CC Utrecht, The Netherlands; [e]Division of Geodynamics, DTU Space, National Space institute, DK-2800 Kgs. Lyngby, Denmark; and [f]Department of Civil, Environmental and Geomatics Engineering, Florida Atlantic University, Boca Raton, FL 33431

Edited* by Ellen S. Mosley-Thompson, The Ohio State University, Columbus, OH, and approved November 17, 2014 (received for review June 23, 2014)

We present a new record of ice thickness change, reconstructed at nearly 100,000 sites on the Greenland Ice Sheet (GrIS) from laser altimetry measurements spanning the period 1993–2012, partitioned into changes due to surface mass balance (SMB) and ice dynamics. We estimate a mean annual GrIS mass loss of 243 ± 18 Gt·y^{-1}, equivalent to 0.68 mm·y^{-1} sea level rise (SLR) for 2003–2009. Dynamic thinning contributed 48%, with the largest rates occurring in 2004–2006, followed by a gradual decrease balanced by accelerating SMB loss. The spatial pattern of dynamic mass loss changed over this time as dynamic thinning rapidly decreased in southeast Greenland but slowly increased in the southwest, north, and northeast regions. Most outlet glaciers have been thinning during the last two decades, interrupted by episodes of decreasing thinning or even thickening. Dynamics of the major outlet glaciers dominated the mass loss from larger drainage basins, and simultaneous changes over distances up to 500 km are detected, indicating climate control. However, the intricate spatiotemporal pattern of dynamic thickness change suggests that, regardless of the forcing responsible for initial glacier acceleration and thinning, the response of individual glaciers is modulated by local conditions. Recent projections of dynamic contributions from the entire GrIS to SLR have been based on the extrapolation of four major outlet glaciers. Considering the observed complexity, we question how well these four glaciers represent all of Greenland's outlet glaciers.

Greenland Ice Sheet | laser altimetry | mass balance | ice dynamics

Comprehensive monitoring of the Greenland Ice Sheet (GrIS) by satellite observations has revealed increasing mass loss since the late 1990s (1, 2), reaching 263 ± 30 Gt·y^{-1} for the period 2005–2010 (3). This translates to a sea level rise (SLR) of 0.73 mm·y^{-1}, about half of which is attributed to a decrease in Surface Mass Balance (SMB) (4) that is expected to continue throughout this century and beyond (5). Over this period, ice dynamic changes contributed about equally to total mass loss, but extrapolating this trend over the next century or two is much more uncertain because of the incomplete understanding of the physical forcing mechanisms responsible for observed flow acceleration and thinning of marine-terminating outlet glaciers. For example, the speedup of Jakobshavn Isbræ, which started in the late 1990s, has been attributed to the disintegration of the floating tongue and loss of buttressing (6), triggered by increased basal melt due to the intrusion of warm water into the fjord (7), or to the weakening of the ice in the lateral shear margins and perhaps a change in the properties at the bed (8).

Acknowledging that such predictions are at a "fairly early stage," the Fifth Assessment Report, issued by the Intergovernmental Panel on Climate Change, includes a projected total SLR by 2100 of 14–85 mm, attributed to dynamic changes of the GrIS for the different future warming scenarios (5). This estimate is based on modeled evolution of four key outlet glaciers (Jakobshavn, Helheim, Kangerlussuaq, and Petermann), whose projected response is scaled up to all Greenland outlet glaciers (9–11). There are two concerns with this approach. First, understanding the dynamic response of marine-terminating outlet glaciers to a warming climate—a prerequisite for deriving reliable mass balance projections—remains a major challenge (12–14). Second, considering the complexity of recent behavior of outlet glaciers (15, 16), it is far from clear how four well-studied glaciers represent all of Greenland's outlet glaciers and whether their response can be scaled up to the entire ice sheet. For example, in southeast Greenland, a region that accounted for more than half of the total 2005 GrIS mass loss (17), many outlet glaciers rapidly adjusted to a new equilibrium by 2006 (16, 18). At the same time, dynamic mass loss continued, or even accelerated, from Jakobshavn Isbræ, the northwest Greenland outlet glaciers and the North East Greenland Ice Stream (19–21).

For improving ice sheet models and sea-level predictions, it is imperative to quantitatively investigate dynamic ice loss processes. Recent results from the Gravity Recovery and Climate Experiment (GRACE) satellite gravimetry (22, 23) and input–output method (IOM, SMB minus discharge) (24) revealed a spatially shifting pattern of annual mass loss during 2003–2010, attributed to a regionally variable interplay of ocean and surface processes as well as ice dynamics. However, the limited spatial resolution of these techniques does not permit documenting the spatial pattern of changes on individual glaciers. Precise elevation measurements, combined with SMB estimates, offer a possibility to increase the spatial resolution of the ice sheet

Significance

We present the first detailed reconstruction of surface elevation changes of the Greenland Ice Sheet from NASA's laser altimetry data. Time series at nearly 100,000 locations allow the characterization of ice sheet changes at scales ranging from individual outlet glaciers to larger drainage basins and the entire ice sheet. Our record shows that continuing dynamic thinning provides a substantial contribution to Greenland mass loss. The large spatial and temporal variations of dynamic mass loss and widespread intermittent thinning indicate the complexity of ice sheet response to climate forcing, strongly enforcing the need for continued monitoring at high spatial resolution and for improving numerical ice sheet models.

Author contributions: B.M.C. designed research; B.M.C., A.F.S., G.B., K.D., S.R., and S.N. performed research; A.F.S., M.R.v.d.B., S.B.S., and J.H.v.A. contributed new data/analytic tools; B.M.C., C.J.v.d.V., G.B., and S.R. analyzed data; and B.M.C., A.F.S., and C.J.v.d.V. wrote the paper.

The authors declare no conflict of interest.

*This Direct Submission article had a prearranged editor.

Freely available online through the PNAS open access option.

[1]To whom correspondence should be addressed. Email: bcsatho@buffalo.edu.

This article contains supporting information online at www.pnas.org/lookup/suppl/doi:10.1073/pnas.1411680112/-/DCSupplemental.

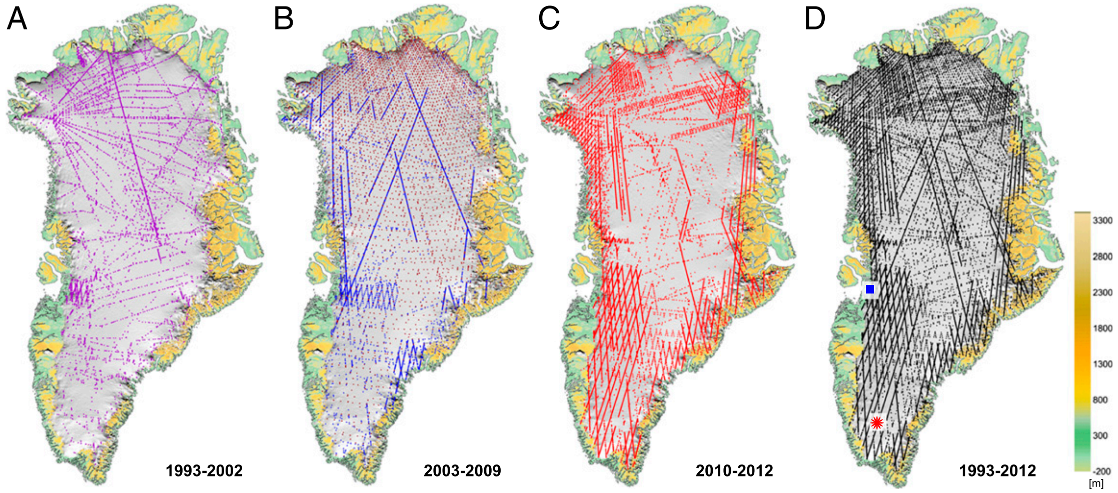

Fig. 1. Location of GrIS elevation time series according to the main data sets used for SERAC reconstruction. (*A*) PARCA ATM (1993–2003) and ICESat (purple); (*B*) PARCA ATM (2003–2009) and ICESat (blue), ICESat crossovers only (brown); (*C*) OIB ATM/LVIS (2009–2012) and ICESat (red); and (*D*) combined: all solutions (black). GrIS is shown in gray, and land surface with local ice caps and glaciers is in green/brown hues. Symbols in *D* mark the locations of elevation change time series shown in Fig. S1.

elevation change and ice dynamics records. Repeat altimetry and stereo imaging have long been used to monitor the cryosphere, mostly for mapping multiyear average elevation changes (2, 25, 26), but neglecting the reconstruction of detailed temporal histories. As surface elevation observations are often collected with varying spatial resolutions and at slightly different locations, the derivation of accurate elevation histories has remained a challenging task.

Here we present, to our knowledge, the first detailed reconstruction of GrIS elevation changes, derived from NASA's 1993–2012 laser altimetry record. Available at nearly 100,000 locations and partitioned into thickness changes associated with SMB variations and dynamic processes, our elevation change history characterizes ice sheet processes on spatial scales ranging from individual outlet glaciers to larger drainage basins and the entire ice sheet. By retaining the original temporal resolution, it is suitable for investigating rapid ice dynamic responses to contemporary atmospheric and oceanic forcings, processes that are still poorly understood (13, 14). Our reconstruction reveals the complexity of ice sheet response to climate forcing. We detect similar, simultaneous elevation changes over distances up to 500 km, indicating climate control on recent mass changes. However, we also show that outlet glacier dynamics exhibits large spatiotemporal variability, suggesting that the response of individual outlet glaciers likely depends on local conditions, such as bed topography and local climate conditions.

Results

Reconstruction of GrIS Elevation Change. As part of NASA's Program for Arctic Regional Climate Assessment (PARCA), airborne laser altimetry surveys began in 1993 with NASA's Airborne Topographic Mapper (ATM) (27). However, investigations of ice sheet mass balance and related sea level rise were hampered by the lack of spatially comprehensive elevation time series. To remedy this, NASA launched the Ice, Cloud and land Elevation Satellite (ICESat) mission in 2003 with the primary goal of measuring elevation changes over the polar ice sheets with sufficient accuracy to assess their impact on global sea level (28). After a successful period of obtaining accurate elevations of the Greenland and Antarctic ice sheets, ICESat's last campaign ended on October 11, 2009. The successor, ICESat-2, is expected to be launched in 2017. To "bridge" the intervening time without satellite laser altimetry data, NASA started Operation IceBridge mission (OIB), which has been gathering laser altimetry data using the ATM and the Land, Vegetation and Ice Sensor [LVIS (29)] airborne systems in both polar regions.

We developed the novel Surface Elevation Reconstruction and Change detection (SERAC) method to determine surface elevation changes at ICESat crossover areas (intersections of ascending and descending ICESat tracks) (30). The method is based on fitting an analytical function to the laser points of a surface patch, such as a crossover area, of $\sim$1 km^2 in size. The surface patches of different time epochs at the same crossover area are related to each other; we have introduced the constraint that within a surface patch, the shape of the ice sheet remains the same over the entire observation period; only its absolute elevation changes. The least-squares adjustment of SERAC simultaneously determines one set of best-fit shape parameters and a time series of elevations for all time epochs involved, together with rigorous error estimates (ref. 30, *SI Text*, and Fig. S1).

Originally limited to ICESat crossover areas only, SERAC has been extended to provide solutions along the ICESat ground tracks by combining ICESat data with airborne laser altimetry data (31). In this way, the spatial density of surface elevation time series increases dramatically, as Fig. 1 vividly demonstrates. Fig. 1*B* depicts ICESat crossover locations (brown) and additional locations where 2003–2009 ATM and LVIS flights intersected or repeated ICESat ground tracks (blue). However, large gaps remain, especially in southern Greenland. Adding ATM data from the period 1993–2002 as well as ATM and LVIS data from 2010 to 2012 remedies this situation, resulting in a dense data set.

The fusion framework of SERAC offers other advantages. For example, inclusion of ATM and/or LVIS data that were collected during ICESat mission (2003–2009) increases the temporal resolution of the elevation change record. If data are available from earlier time periods, the time series are extended backward in time, before 2003. Using data from the OIB mission extends the time series toward the present.

Ultimately, by combining all NASA laser altimetry measurements, elevation time series are reconstructed at $\sim$100,000 locations, resulting in a very dense coverage along ICESat ground tracks, especially in the ice sheet marginal region. Despite occasional cloud cover, ice sheet elevations were measured at least once during each of the 19 ICESat operational periods at most crossover locations (30). Thus, by adding ATM and LVIS

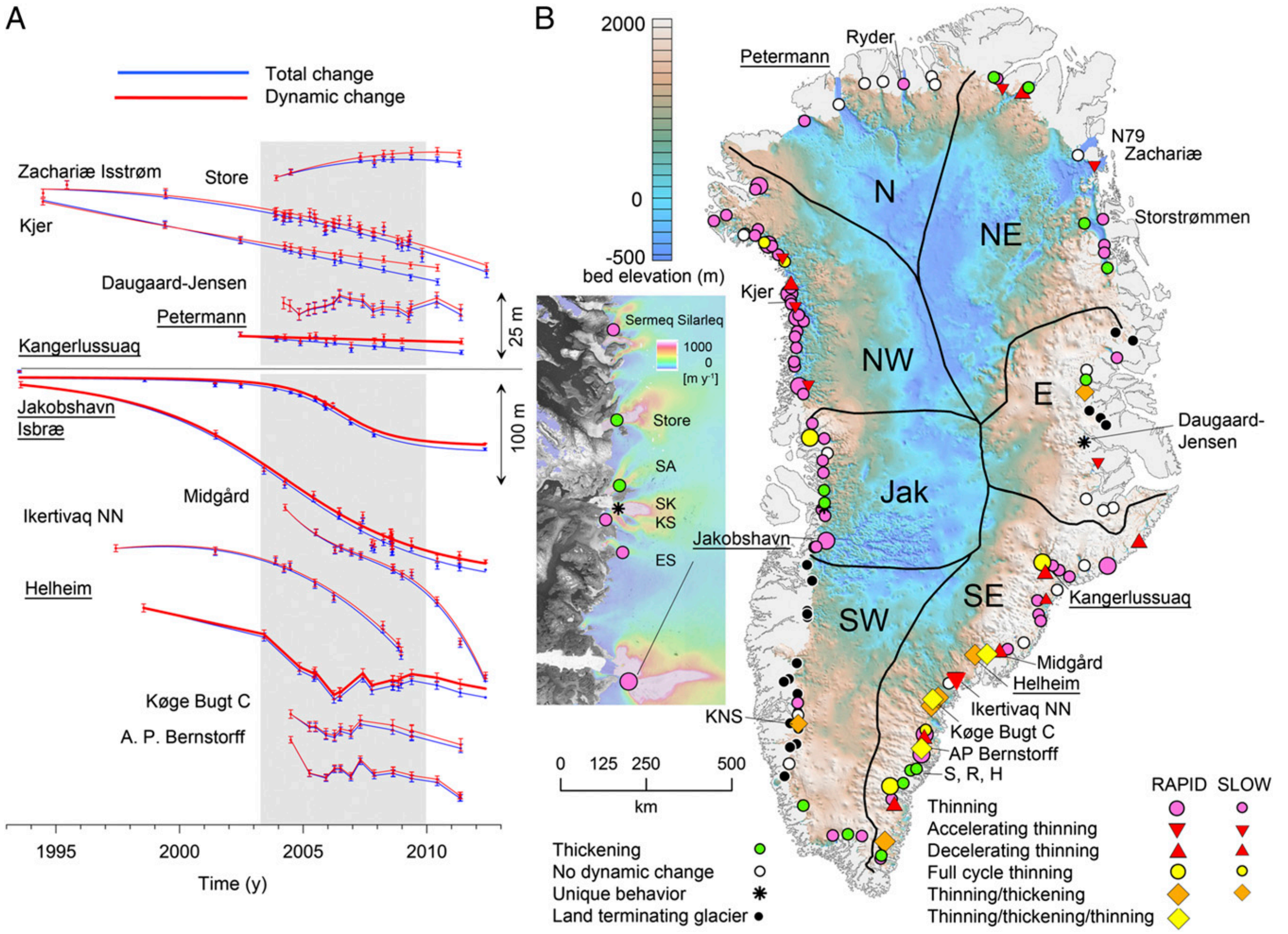

Fig. 2. Classification of outlet glaciers based on dynamic thickness change pattern. (*A*) Thickness change time series derived from the combined ICESat/ATM/LVIS altimetry record (1993–2012) illustrating different dynamic outlet glacier behaviors. Thickening: Store Glacier (6); no dynamic change: Petermann Glacier (78); decelerating thinning: Kjer Glacier (83); accelerating thinning: Zachariæ Isstrom (51) and Ikertivaq NN (46); full cycle thinning: Jakobshavn Isbræ (1); thinning with varying rate: Midgård Glacier (121); thinning, thickening, and thinning with abrupt termination of initial thinning: Helheim (3), Koge Bugt C (4), and A. P. Bernstorff (12) glaciers; unique pattern with periodic thinning and thickening: Daugaard-Jensen Glacier (8). Numbers in parentheses are ID numbers from ref. 32 and in Table S1. Gray box marks the duration of the ICESat mission, and glacier locations are shown in *B*. Dynamic thickness changes of the four large outlet glaciers, Jakobshavn Isbræ, Kangerlussuaq, Helheim, and Petermann glaciers, underlined in the figure, are modeled in refs. 9–11. (*B*) Distribution of different outlet glacier behavior types over a background of ice sheet bed elevation from ref. 45. *Inset* shows the detailed pattern north of Jakobshavn Isbræ overlain on ice velocities from ref. 32. Abbreviations mark the following outlet glaciers: Sermeq Avannarleq (SA, 53), Sermeq Kujalleq (SK, 13), Kangilerngata Sermia (KS, 52), Eqip Sermia (ES, 90), Kangiata Nunaata Sermia (KNS, 36), Skinfaxe (S, 82), Rimfaxe (R, 58), and Heimdal (H, 39) glaciers. See Table S1 for a complete list of glaciers and their classification based on 2003–2009 and 1993–2012 dynamic thickness change patterns.

measurements, a dense temporal sampling is obtained for 2003–2009, with additional points from LVIS and ATM extending most of the curves beyond ICESat's lifetime (Fig. 2*A* and Fig. S1). After removing the effect of vertical crustal motion due to Glacial Isostatic Adjustment (GIA; *SI Text*), we partition the ice thickness change time series into components associated with ice dynamics and SMB changes (*Materials and Methods*, *SI Text*, and Fig. S1).

The high spatial density of the new 1993–2012 elevation change record and the 91-d repeat cycle of ICESat allow for the investigation of the spatiotemporal pattern of ice sheet thickness change at different scales. The ice thickness change time series (Fig. 2*A* and Fig. S1) provides the highest resolution, suitable for characterizing the dynamic processes affecting individual outlet glaciers. The most recent compilation of GrIS ice velocities includes 242 outlet glaciers with a width greater than 1.5 km (32). We identified 130 of these glaciers with a 5- to 19-y-long altimetry record, out of which 115 are marine terminating (Tables S1 and S2). Average elevation change rates are found to be in good agreement with previous studies (*SI Text* and Table S3). However, we have shown that changes are typically nonlinear in time and most of the rapid changes occur during the ICESat mission (Fig. 2*A*). For many marine-terminating outlet glaciers, dynamic thickness change patterns are consistent with an inland propagation of dynamic thinning or thickening initiated at the coast (Fig. S2 *A* and *B*). Some glaciers exhibit a more complicated behavior, however. For example, Størstrommen, L. Bistrup Bræ, and Marie Sophie glaciers, which are quiescent surging glaciers, have a characteristic pattern with large, steady thickening at their source regions, as ice accumulates upstream of the reduced flow, and thinning below the area where the surge was initiated (Fig. S2*C* and Table S1), while the complex elevation change pattern of Hagen Bræ might indicate an ongoing surge (Table S1). Short-term, sometimes cyclic elevation changes occurred on 15 outlet glaciers, all marine terminating (*SI Text* and Table S1), and may indicate control from subglacial hydrology or are perhaps related to the drainage of proglacial lakes (e.g., Daugaard-Jensen Glacier, Fig. S2*D*). Dynamic thinning was negligible on 13 out of the 15 land-terminating glaciers (*SI Text* and Tables S1 and S2).

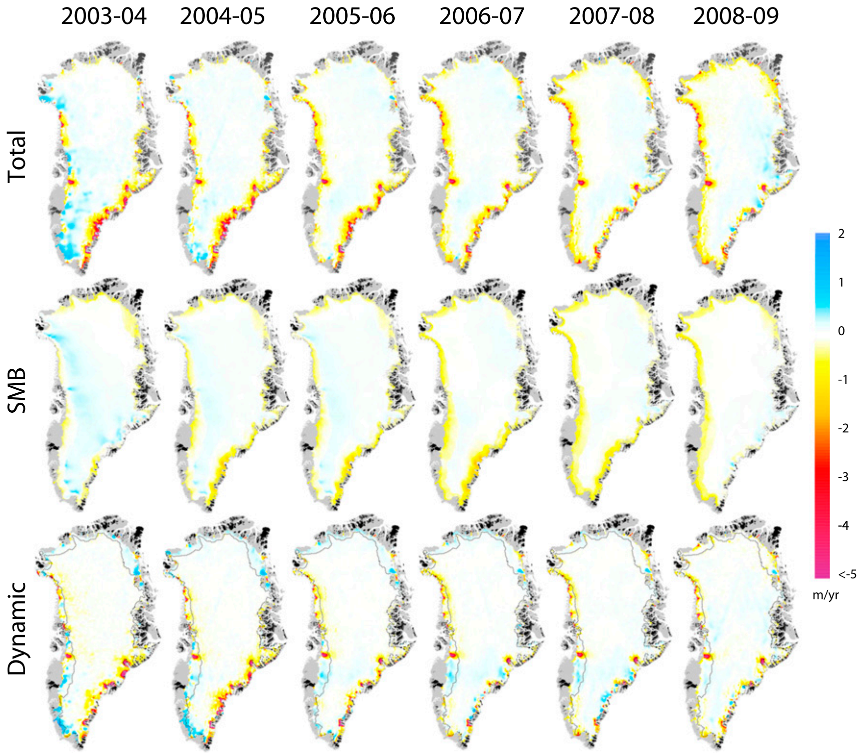

Fig. 3. Annual total, SMB-related, and ice dynamics-related thickness change rates of the GrIS for 2003–2009 balance years from ICESat, ATM and LVIS laser altimetry observations (see Fig. 1 for locations of elevation change records). Dotted lines on the dynamic thickness change maps mark the ELA (average 2003–2009 SMB = 0). Ice sheet boundary is from ref. 46, and black regions show weakly or not connected glaciers and ice caps. Balance years start on September 1 and end on August 31 of the following year. See Movie S1 for a higher-resolution, animated version of the figure.

To facilitate interpretation, glaciers are divided into the following distinct groups according to their dynamic thickness change pattern in 2003–2009: thinning with steady or slowly changing rates (accelerating, decelerating, full cycle thinning); slow or rapid thinning that abruptly terminated and was followed by thickening and in some cases by resumed thinning; thickening; unique elevation change pattern; and no dynamic change (Fig. 2 and Table S1).

To investigate drainage basin-scale processes, we compute annual ice thickness change rates at each surface patch location from a polynomial fit through the thickness changes reconstructed by SERAC (30) and partition these rates into changes associated with SMB and ice dynamics (*Materials and Methods*, *SI Text*, and Fig. S1). The interpolated annual thickness change rate grids show intricate and rapidly changing patterns (Fig. 3 and Movie S1). To quantify these, volume and mass change rates of the main ice sheet regions are calculated (Fig. 4 and Tables S4 and S5).

GrIS Ice Thickness Change and Mass Loss Patterns, 1993–2012. We estimated a mean annual GrIS loss of 243 ± 18 $\mathrm{Gt \cdot y^{-1}}$ (277 ± 7 $\mathrm{km^3 \cdot y^{-1}}$), equivalent to 0.68 ± 0.05 $\mathrm{mm \cdot y^{-1}}$ SLR for 2003–2009 (Tables S4 and S5). This mass loss and its interannual variability are in good agreement with the reconciled GrIS mass loss estimate derived from a combined ensemble of laser altimetry, GRACE, and IOM data (3). However, we detected higher average mass loss and interannual variability than the laser altimetry results included in ref. 3, bringing the laser altimetry, GRACE, and IOM estimates closer to each other (ref. 3, *SI Text*, and Tables S5 and S6), thus reconciling the previously perceived inconsistencies among different methods. Dynamic thinning contributed 48% to the total mass loss, which is the same as reported in ref. 4. Dynamic loss was largest in 2004–2005, followed by a gradual decrease that was balanced by accelerating SMB loss (Fig. 4). However, at the same time, the relative contributions of major drainage basins changed significantly (Figs. 3 and 4), indicating that processes acting on time scales of less than a decade have a significant effect on ice sheet mass loss and related SLR. The only region exhibiting steady mass loss from 2003 to 2009 was Jakobshavn, while mass loss decelerated from southeast and east Greenland and accelerated from the rest of Greenland, confirming the pattern reconstructed from GRACE observations (23). In this section, we review the dynamic behavior of individual marine-terminating outlet glaciers and explore their impact on drainage basin scale dynamic mass changes.

Almost half of the total 2003–2009 GrIS mass loss originated from southeast Greenland (Table S5). Glaciers in this sector thinned rapidly between 2003 and 2005, reaching their peak discharge in 2005 (refs. 16 and 18, Figs. 3 and 4). During this time, dynamic thinning extended far inland, up to the ice divide in some areas (Movie S1), maintaining a pattern that started in the 1970s or earlier (33). This large dynamic loss, peaking at 166 ± 31 $\mathrm{Gt \cdot y^{-1}}$, was a major source of the record negative GrIS mass balance of 293 ± 38 $\mathrm{Gt \cdot y^{-1}}$ in 2004–2005. As flow acceleration slowed down or reversed to deceleration after 2005 (16), thinning rates decreased, and several glaciers, for example Helheim Glacier, started to thicken (Fig. 2). At the same time, the long-term trend of high-elevation thinning also reversed, and by 2007–2008, most of southeast GrIS exhibited dynamic thickening (Fig. 3 and Movie S1). By 2007–2008, the ice loss rate from the southeast GrIS dropped to less than one third of its peak value, as a result of a diminishing dynamic mass loss. However, the slowdown and thickening of outlet glaciers was short lived, as they resumed acceleration (16) and thinning by 2009 (Fig. 2). In addition to widespread short-term changes, outlet glacier thinning shows a large spatial variability in southeast Greenland, much like the velocity record (16), indicating an intricate interplay of regional and local forcings and controls. For example, rapid thickening of outlet glaciers within a region extending to 500 km in north–south direction, and including Helheim, Køge Bugt C, and A. P. Bernstorff glaciers, started at the same time and exhibited very similar patterns (Fig. 2), suggesting regional climate controls. Meanwhile, other glaciers in the region, such as Midgård and Ikertivaq glaciers, continued to thin, losing

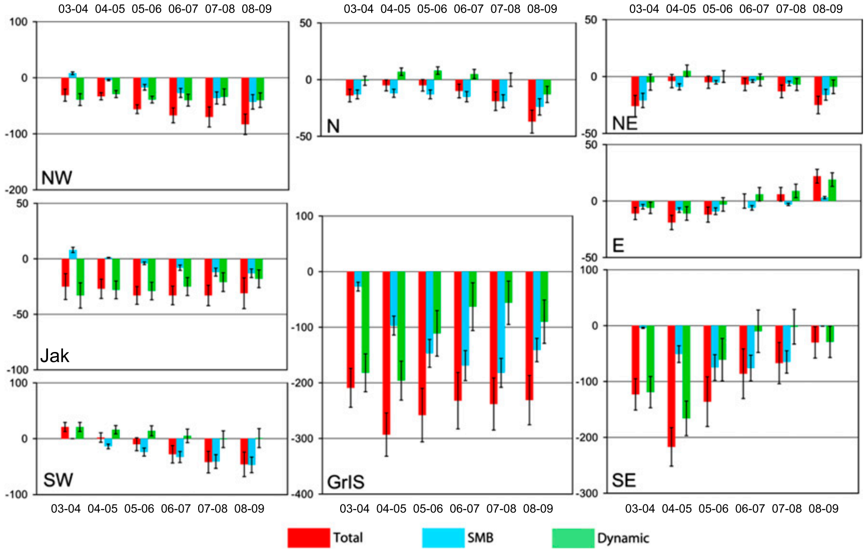

Fig. 4. Annual mass change rates in gigatons per year for major drainage basins shown in Fig. 2*B*. Annual total mass change rates from laser altimetry (red) are partitioned into mass changes due to SMB (blue) and ice dynamics (green). Annual mass change rates and their error estimates are listed in Table S5.

ice at increasing rates. In contrast, Heimdal, Rimfaxe, and Skinfaxe glaciers, maintaining steady calving front positions since 1933 (34), have been thickening (Fig. 2*B*).

Concurrent with the 2003–2005 rapid thinning of the southeast region, the adjacent southwest basin was thickening (Fig. 3 and Movie S1). This positive mass balance was due to the dynamic thickening of the land-terminating ice sheet margin, interpreted as a reaction to increasing accumulation during an ice sheet readvance 4,000 y ago (35). Increasing dynamic thinning of major outlet glaciers (e.g., Kangiata Nunata Sermia, Fig. 2*B*) and accelerating SMB loss resulted in an overall negative mass balance of this region by 2005 (Fig. 4).

Annual mass loss of the Jakobshavn region was steady at a rate of 30 ± 4 $\mathrm{Gt \cdot y^{-1}}$, dominated by losses caused by the continuing speedup and corresponding thinning of Jakobshavn Isbræ (19). Thinning rates started to decrease near its calving front in 2007 (Fig. 2*A* and Fig. S2*A*), indicating an adjustment to new environmental conditions and signaling a potential future mass loss decrease. The outlet glaciers draining to the narrow fjords north of Jakobshavn Isbræ show a complex spatial pattern of dynamic elevation changes in 2003–2009 (Fig. 2*B*, *Inset*).

In northwest Greenland, ice loss has accelerated linearly from 31 ± 11 $\mathrm{Gt \cdot y^{-1}}$ to 83 ± 18 $\mathrm{Gt \cdot y^{-1}}$ between 2003 and 2009, due to increasingly negative SMB anomalies and a steady dynamic loss (Fig. 4 and Table S5). Our long-term altimetry record shows that dynamic thinning has been steady or accelerated on most outlet glaciers during the last 15–20 y (e.g., Kjer Glacier, Fig. 2). This is consistent with the steady increase of ice discharge between 2000 and 2010 detected by refs. 16 and 36 and contradicts a previous reconstruction that indicated a stable period between 1992 and 2005, followed by dynamic thinning and increased discharge (37).

The three other major regions (north, east, and northeast) remained dynamically relatively inactive over the period of 2003–2009. Ice sheet mass balance had a similar trend in north and northeast, where a decreasing negative balance was followed by a slow mass loss increase since 2005 due to a combination of increasing negative SMB and increasing dynamic loss. Thinning rates of north and northeast Greenland outlet glaciers are relatively small (<5 $\mathrm{m \cdot y^{-1}}$). However, thinning of Ryder Glacier and Zachariæ Isstrom (Fig. 2) at current or increasing rates could unground their large ice plains within a few decades as continuing thinning brings the ice closer to flotation (21, 26). The resulting speedup over large areas would ultimately cause a significant mass loss from the deep central part of the GrIS. Elevation changes were also small, but increasingly positive, in east Greenland, resulting in a positive mass balance by 2007.

Discussion

The spatiotemporal pattern of annual ice sheet thickness change rates shows clear trends as well as interannual variations (Fig. 3). Averaged over the entire GrIS, the central, high-elevation part was slightly thickening during the entire time, with interannual variations corresponding to SMB anomalies. Dynamic thinning was most pronounced below the equilibrium line altitude (ELA), with the largest thinning rates observed on Jakobshavn, Helheim, and Kangerlussuaq glaciers and in southeast and northwest Greenland. The dynamic behavior of dominant outlet glaciers determines the mass loss pattern of major drainage basins (Figs. 2 and 4). Dynamic mass loss and gain varied rapidly in southeast Greenland where most glaciers, fed by short and narrow drainage basins and reaching the fjords through narrow and deep bedrock channels, appear to adjust in 3–4 y to changing boundary conditions. In contrast, most outlet glaciers in northwest Greenland have been exhibiting uninterrupted long-term dynamic thinning, in some cases for more than 15 y (e.g., Kjer Glacier, Fig. 2). Here, outlet glaciers drain a 50- to 80-km-wide coastal region with deep channels incised into a relatively flat topography only slightly above sea level, facilitating a rapid propagation of outlet glacier thinning to the surrounding slower flowing regions.

Dynamic thinning of outlet glaciers exhibits a large spatial and temporal variability (Fig. 2, *SI Text*, and Tables S1 and S2). Different glacier groups are not confined to specific regions, and some nearby outlet glaciers show very different temporal behavior. This casts doubt on models that attribute observed flow accelerations and thinning to a single mechanism. Rather, these observations suggest that response of individual glaciers to external forcings is more involved and may depend on local geometry factors such as bed topography and size of the drainage basin. The rapid reversal of thinning to thickening in southeast Greenland over a region that extends far inland suggests that mass changes might occur in response to processes acting over larger areas, rather than near the grounding line only. This behavior has not been captured in existing ice flow models and may be linked to rapid changes in subglacial hydrology affecting the sliding speed (38, 39). The majority of GrIS mass loss during the period of 2003–2009 is due to thinning of southeast and northwest Greenland glaciers with small to moderately sized drainage basins, rather than the four large modeled glaciers (Fig. S3*A*). Moreover, mass loss is not proportional with drainage basin area (Fig. S3*B*), as was assumed by ref. 10. These findings challenge the practice of estimating the future dynamic contribution of the entire GrIS to global sea level based on modeled behavior of three or four major outlet glaciers, one of which (Petermann Glacier) did not show much dynamic change over the period considered.

Our record shows that continuing dynamic thinning provides a substantial contribution to Greenland mass loss. The large spatial and temporal variations of dynamic mass loss and widespread intermittent thinning indicate the complexity of ice sheet response to climate forcing, pointing to the need for continued monitoring of the GrIS at high spatial resolution.

Materials and Methods

Elevation change time series are reconstructed from ICESat, ATM, and LVIS laser altimetry data by SERAC (see *SI Text* for details on the data sets and their accuracies). They are corrected for GIA and partitioned into components corresponding to SMB anomalies, changes in firn compaction rates, and ice dynamics (Fig. S1). GIA-related vertical crustal motion estimates are from ref. 40. Regional Atmospheric Climate Model (RACMO2/GR) SMB anomalies (41) are converted into ice thickness change using surface firn densities derived by a simple empirical model (42). This model accounts for the formation of ice lenses in the snowpack assuming that all retained meltwater refreezes at the same annual layer. Variations of firn compaction rates are from a 5-km by 5-km gridded model (43) forced by the output from the HIRHAM5 Regional Climate Model (44). Annual rates of total, SMB-related, and dynamic ice thickness change rates are estimated from polynomial approximations of the time series, and are gridded into 2-km-resolution grids using ordinary kriging with an exponential, isotropic variogram model. To obtain mass changes, we converted dynamic thickness changes to mass changes with an assumed ice density of 917 $\mathrm{kg \cdot m^{-3}}$. Total mass changes were then estimated as the sum of dynamic and SMB mass changes. Details on the computation of the total, SMB, and dynamic thickness change time series, as well as thickness, volume, and mass change rates, together with their error estimates, are presented in *SI Text*. Comparison with published thickness change rates (Table S3) and mass balance rate estimates (Table S6) confirms the accuracy of our results.

ACKNOWLEDGMENTS. ICESat, ATM, and LVIS data were collected by NASA's PARCA, ICESat, and OIB missions and distributed by the National Snow and Ice Data Center. B.M.C., A.F.S., C.J.v.d.V., K.D., G.B., S.R., and S.N. acknowledge support by NASA's Polar Program under Grants NNX10AV13G, NNX11AR23G, and NNX12AH15G. M.R.v.d.B. and J.H.v.A. acknowledge support from the Netherlands Polar Program of Netherlands Organization for Scientific Research Division for the Earth and Life Sciences (NWO-ALW) and EU FP7 program ice2sea.

1. Rignot E, Velicogna I, van den Broeke MR, Monaghan A, Lenaerts J (2011) Acceleration of the contribution of the Greenland and Antarctic ice sheets to sea level rise. *Geophys Res Lett* 38(5):L05503.
2. Zwally HJ, et al. (2011) Greenland ice sheet mass balance: Distribution of increased mass loss with climate warming; 2003-07 versus 1992-2002. *J Glaciol* 57(201):88–102.
3. Shepherd A, et al. (2012) A reconciled estimate of ice-sheet mass balance. *Science* 338(6111):1183–1189.
4. van den Broeke M, et al. (2009) Partitioning recent Greenland mass loss. *Science* 326(5955):984–986.
5. Church JA, et al. (2013) Sea level change. *Climate Change 2013: The Physical Science Basis. Contribution of Working Group I to the Fifth Assessment Report of the Intergovernmental Panel on Climate Change*, eds Stocker TF, et al. (Cambridge Univ Press, New York), pp 1137–1216.
6. Joughin I, et al. (2008) Continued evolution of Jakobshavn Isbrae following its rapid speedup. *J Geophys Res* 113(F4):F04006.
7. Holland DM, Thomas RH, De Young B, Ribergaard MH, Lyberth B (2008) Acceleration of Jakobshavn Isbrtriggered by warm subsurface ocean waters. *Nat Geosci* 1(10):659–664.
8. van der Veen CJ, Plummer JC, Stearns LA (2011) Controls on the recent speed-up of Jakobshavn Isbræ, West Greenland. *J Glaciol* 57(204):770–782.
9. Price SF, Payne AJ, Howat IM, Smith BE (2011) Committed sea-level rise for the next century from Greenland ice sheet dynamics during the past decade. *Proc Natl Acad Sci USA* 108(22):8978–8983.
10. Nick FM, et al. (2013) Future sea-level rise from Greenland's main outlet glaciers in a warming climate. *Nature* 497(7448):235–238.
11. Goelzer H, et al. (2013) Sensitivity of Greenland ice sheet projections to model formulations. *J Glaciol* 59(216):733–749.
12. Joughin I, Alley RB, Holland DM (2012) Ice-sheet response to oceanic forcing. *Science* 338(6111):1172–1176.
13. Straneo F, et al. (2013) Challenges to understanding the dynamic response of Greenland's marine terminating glaciers to oceanic and atmospheric forcing. *Bull Am Meteorol Soc* 94(8):1131–1144.
14. Straneo F, Heimbach P (2013) North Atlantic warming and the retreat of Greenland's outlet glaciers. *Nature* 504(7478):36–43.
15. McFadden EM, Howat IM, Joughin I, Smith BE, Ahn Y (2011) Changes in the dynamics of marine terminating outlet glaciers in west Greenland (2000–2009). *J Geophys Res* 116(F2):F02022.
16. Moon T, Joughin I, Smith B, Howat I (2012) 21st-century evolution of Greenland outlet glacier velocities. *Science* 336(6081):576–578.
17. Rignot E, Kanagaratnam P (2006) Changes in the velocity structure of the Greenland Ice Sheet. *Science* 311(5763):986–990.
18. Howat IM, Joughin I, Scambos TA (2007) Rapid changes in ice discharge from Greenland outlet glaciers. *Science* 315(5818):1559–1561.
19. Howat IM, et al. (2011) Mass balance of Greenland's three largest outlet glaciers, 2000–2010. *Geophys Res Lett* 38(12):L12501.
20. Khan SA, Wahr J, Bevis M, Velicogna I, Kendrick E (2010) Spread of ice mass loss into northwest Greenland observed by GRACE and GPS. *Geophys Res Lett* 37(6):L06501.
21. Khan SA, et al. (2014) Sustained mass loss of the northeast Greenland ice sheet triggered by regional warming. *Nat Clim Change* 4(4):292–299.
22. Harig C, Simons FJ (2012) Mapping Greenland's mass loss in space and time. *Proc Natl Acad Sci USA* 109(49):19934–19937.
23. Luthcke SB, et al. (2013) Antarctica, Greenland and Gulf of Alaska land-ice evolution from an iterated GRACE global mascon solution. *J Glaciol* 59(216):613–631.
24. Sasgen I, et al. (2012) Timing and origin of recent regional ice-mass loss in Greenland. *Earth Planet Sci Lett* 333:293–303.
25. Pritchard HD, Arthern RJ, Vaughan DG, Edwards LA (2009) Extensive dynamic thinning on the margins of the Greenland and Antarctic ice sheets. *Nature* 461(7266):971–975.
26. Thomas R, Frederick E, Krabill W, Manizade S, Martin C (2009) Recent changes on Greenland outlet glaciers. *J Glaciol* 55(189):147–162.
27. Krabill WB, et al. (2002) Aircraft laser altimetry measurement of elevation changes of the Greenland ice sheet: Technique and accuracy assessment. *J Geodyn* 34(3):357–376.
28. Zwally HJ, et al. (2002) ICESat's laser measurements of polar ice, atmosphere, ocean, and land. *J Geodyn* 34(3):405–445.
29. Hofton MA, Blair JB, Luthcke SB, Rabine DL (2008) Assessing the performance of 20–25 m footprint waveform lidar data collected in ICESat data corridors in Greenland. *Geophys Res Let* 35(24):L24501.
30. Schenk T, Csathó B (2012) A new methodology for detecting ice sheet surface elevation changes from laser altimetry data. *IEEE Trans Geosci Remote Sens* 50(9):3302–3316.
31. Schenk T, Csatho B, van der Veen C, McCormick D (2014) Fusion of multi-sensor surface elevation data for improved characterization of rapidly changing outlet glaciers in Greenland. *Remote Sens Environ* 149:239–251.
32. Rignot E, Mouginot J (2012) Ice flow in Greenland for the International Polar Year 2008–2009. *Geophys Res Lett* 39(11):L11501.
33. Thomas R, et al. (2001) Mass balance of higher-elevation parts of the Greenland ice sheet. *J Geophys Res* 106(D24):33707–33716.
34. Bjørk AA, et al. (2012) An aerial view of 80 years of climate-related glacier 278 fluctuations in southeast Greenland. *Nat Geosci* 5(6):427–432.
35. Huybrechts P (1994) The present evolution of the Greenland ice sheet: An assessment by modelling. *Global Planet Change* 9(1):39–51.
36. Enderlin EM, et al. (2014) An improved mass budget for the Greenland ice sheet. *Geophys Res Lett* 41(3):866–872.
37. Kjær KH, et al. (2012) Aerial photographs reveal late-20th-century dynamic ice loss in northwestern Greenland. *Science* 337(6094):569–573.
38. Schoof C (2010) Ice-sheet acceleration driven by melt supply variability. *Nature* 468(7325):803–806.
39. Koenig LS, Mige C, Forster RR, Brucker L (2014) Initial in situ measurements of perennial meltwater storage in the Greenland firn aquifer. *Geophys Res Lett* 41(1):81–85.
40. G A, Wahr J, Zhong S (2013) Computations of the viscoelastic response of a 3-D compressible Earth to surface loading: An application to Glacial Isostatic Adjustment in Antarctica and Canada. *Geophys J Int* 192(2):557–572.
41. van Angelen JH, van den Broeke MR, Wouters B, Lenaerts JTM (2014) Contemporary (1960–2012) evolution of the climate and surface mass balance of the Greenland ice sheet. *Surv Geophys* 35(5):1155–1174.
42. Reeh N, Fisher DA, Koerner RM, Clausen HB (2005) An empirical firn-densification model comprising ice lenses. *Ann Glaciol* 42(1):101–106.
43. Sørensen LS, et al. (2011) Mass balance of the Greenland ice sheet (2003–2008) from ICESat data – the impact of interpolation, sampling and firn density. *Cryosphere* 5(1):173–186.
44. Lucas-Picher P, et al. (2012) Very high resolution regional climate model simulations over Greenland: Identifying added value. *J Geophys Res* 117(D2):D02108.
45. Bamber JL, et al. (2013) A new bed elevation dataset for Greenland. *Cryosphere* 7(2):499–510.
46. Rastner P, Bolch T, Molg N, Machguth H, Paul F (2012) The first complete glacier inventory for the whole of Greenland. *Cryosphere* 6(4):1483–1495.